Article:
Browning, KA, Marsham, JH, White, BA et al. (1 more author) (2012) A case study of a large patch of billows surmounted by elevated convection. Quarterly Journal of the Royal Meteorological Society, 138 (668). 1764 - 1773. ISSN 0035-9009

https://doi.org/10.1002/qj.1908

RMetS
Royal Meteorological Society

A case study of a large patch of billows surmounted by elevated convection

K. A. Browning,[a] J. H. Marsham,[b]* B. A. White[a] and J. C. Nicol[c]
[a]*School of Earth and Environment, University of Leeds, UK*
[b]*National Centre of Atmospheric Science (NCAS), University of Leeds, UK*
[c]*National Centre of Atmospheric Science (NCAS), University of Reading, UK*

*Correspondence to: J. Marsham, Institute for Climate and Atmospheric Science, School of Earth and Environment, University of Leeds, Woodhouse Lane, Leeds LS2 9JT, UK. E-mail: jmarsham@env.leeds.ac.uk

A region of large-amplitude Kelvin-Helmholtz billows, of area 2000 km^2, was observed in a region of moderate rain at the rear of a mesoscale convective system on a day during the Convective Storm Initiation Project in southern England. The mesoscale convective system (MCS) was characterized by elevated convection above a layer of cool air, separated by a sloping statically stable layer characterized by strong wind shear. Doppler radar observations showed that the large patch of billows was situated within this shear layer and that it persisted over the 2 h period of observation, maintaining its position with respect to the MCS and producing surface pressure perturbations of $\pm$ 0.3 hPa. Potentially unstable air above the sloping shear layer reached its level of free convection while ascending above this layer. The resulting elevated convection was in the form of cells whose spacing appeared to be influenced by the underlying billows. Results from large-eddy model simulations are shown to support the hypothesis that, although the large-scale ascent alone would have triggered the elevated convection, the billows exerted a secondary forcing effect on the convection.

Key Words: mesoscale convective system; elevated convection; Kelvin-Helmholtz instability; Doppler radar; large-eddy model; Convective Storm Initiation Project

Received 10 November 2011; Revised 18 January 2012; Accepted 30 January 2012; Published online in Wiley Online Library 1 March 2012

Citation: Browning KA, Marsham JH, White BA, Nicol JC. 2012. A case study of a large patch of billows surmounted by elevated convection. *Q. J. R. Meteorol. Soc.* **138**: 1764–1773. DOI:10.1002/qj.1908

1. Introduction

Billows are a form of breaking waves caused by shearing instability within statically stable layers of the atmosphere. Known as Kelvin–Helmholtz (KH) billows, they are important both as a source of turbulence and as a mechanism for the vertical transport of heat, mass and momentum. There have been many studies of KH billows, both in the clear air, where they are responsible for clear air turbulence (CAT), and in cloud and precipitation. Recent examples of situations in which billows were observed within precipitation include the studies of a wintertime storm by Houser and Bluestein (2011) and of a summertime mesoscale convective system (MCS) by Browning *et al.* (2010) and Marsham *et al.* (2010). Sometimes the statically stable layer within which the billows form is surmounted by a nearly saturated, potentially unstable layer, giving rise to elevated convection. This was so on the occasion studied by Browning *et al.* (2010) and Marsham *et al.* (2010). They focused on a single intense MCS for which the billows appeared to be a secondary issue; however, another MCS on the same day was associated with a large coherent patch of billows that appeared to be interacting with overlying elevated convection. This kind of interaction has received little, if any, attention in the past and is the focus of the present study.

The large patch of KH billows analysed here was in a region of moderate rainfall intensity at the rear of an MCS that was observed in southern England on

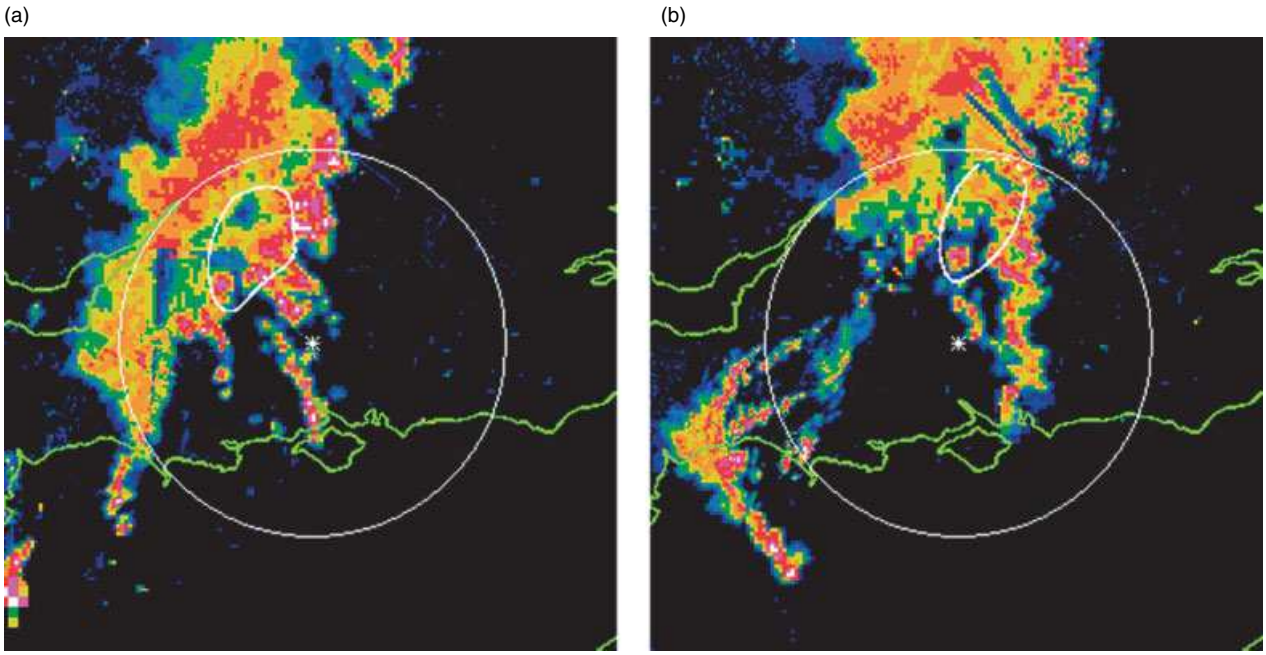

Figure 1. Rain echo pattern in southern England and Wales, obtained from the operational weather radar network at (a) 0945 and (b) 1045 UTC, 24 June 2005. Colours represent rain rates from <0.5 mm h^{-1} (blue), doubling with each colour step to >8 mm h^{-1} (red), >16 (purple) and >32 mm h^{-1} (white), retrieved assuming $Z = 200\,R^{1.6}$ (Harrison *et al.*, 1998). The circle shows the 95 km radius coverage of the Chilbolton radar (not one of the network radars). The line of intense convective echoes extending north–south through Chilbolton at 0945 corresponds to the leading edge of MCS B. The roughly elliptical contour behind the main rain area of MCS B shows the extent of the patch of large-amplitude billows inferred from Figure 2. A further area of rain associated with another, weakening, MCS is located to the northwest of the patch of billows.

24 June 2005 during IOP (intensive observation period) 3 of the Convective Storm Initiation Project (CSIP). The observational facilities available during CSIP have been described by Browning *et al.* (2007) but the only data used in the present study were those from the high-resolution (0.28° half-power beam width), 10 cm wavelength Chilbolton Doppler radar (Goddard *et al.*, 1994), the operational weather radar network, and also one of the automatic weather stations (AWSs) and a special radiosonde ascent, both close to the billow event. The observations indicate that the billows may have had a forcing effect on the overlying convection (sections 2 and 3). Simulations from a large-eddy model are used to support this interpretation (section 4).

2. Observed structure and behaviour of the patch of billows

2.1. Location and extent of the billows

The billows analysed in this paper occurred during the morning on 24 June 2005. A shallow low was situated just to the south, over the north coast of France, and southern England was affected by a cool north to northeasterly flow. This was overridden by a flow at higher levels from between the south and southwest. The billows were situated in the sheared transition zone between these two flows. Rain was widespread in association with a series of MCSs that developed ahead of a cold front. Figure 1 shows radar network composite images giving the pattern of rainfall at 0945 and 1045 (all times are UTC) on 24 June 2005. The area covered is centred on the radar at Chilbolton in southern England. The circle is at a range of 95 km from Chilbolton. Several MCSs are depicted in this figure. The MCS analysed by Browning *et al.* (2010) and Marsham *et al.* (2010), which they designated MCS C, is the one in the bottom left-hand

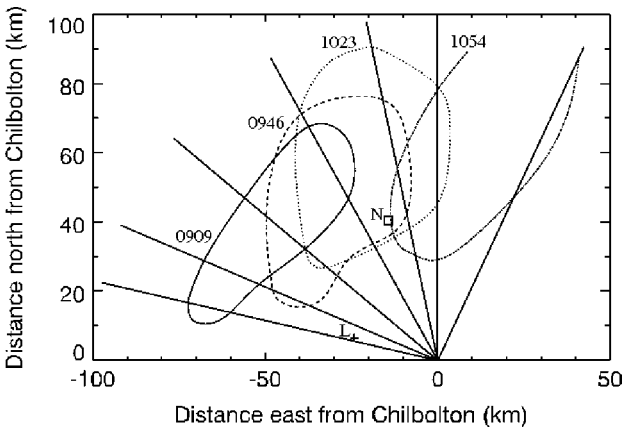

Figure 2. Contours showing the approximate extent of the large-amplitude billows at times centred on 0909, 0946, 1023 and 1054 UTC, as derived from RHI scans along the radials indicated. The locations of the automatic weather station (at North Farm) and the radiosonde station (at Larkhill) are labelled N and L, respectively.

corner, mostly beyond the range circle during this period. The billows analysed in the present paper were associated with an earlier MCS, referred to as MCS B. The leading edge of MCS B was characterized by the north–south line of heavy-rain cells that reached Chilbolton at 0945 (Figure 1(a)).

Figure 2 shows a set of four envelopes representing the approximate extent of the billow patch centred at times 0909, 0946, 1023 and 1054, as derived from 4 cycles of range–height indicator (RHI) scans with the Chilbolton radar along the radials indicated. Data from one of the RHI scans showing billows are presented shortly, in section 2.2. The discrimination between billows and no billows is somewhat fuzzy and so the precise position of the boundary

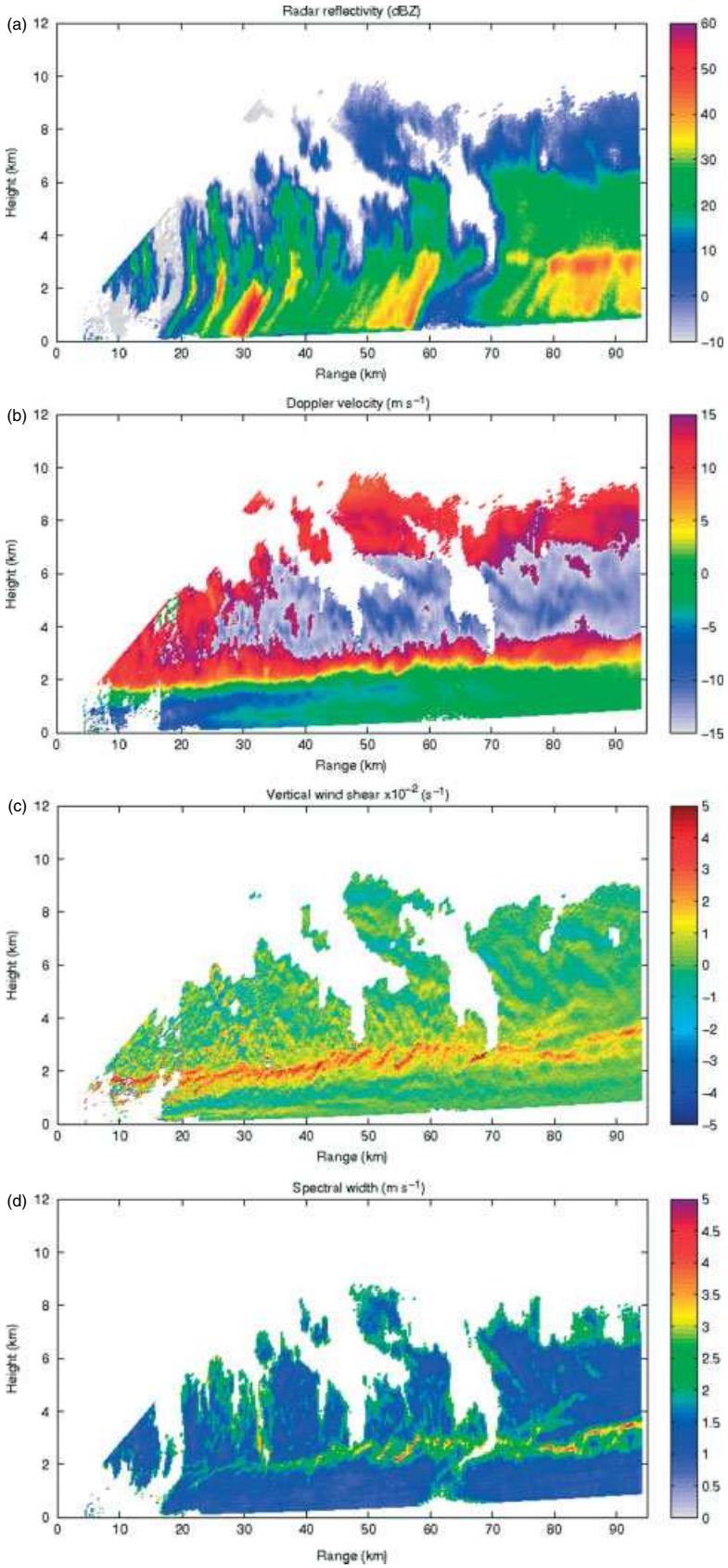

Figure 3. RHI scan from the Chilbolton radar along 348° at 1023 UTC, 24 June 2005, showing (a) reflectivity, (b) Doppler velocity (velocities are 'folded' such that the upper-level grey and blue areas represent positive velocities greater than 15 m s^{-1}), (c) vertical shear of the Doppler velocity and (d) spectral width. Heights are shown above the radar dish (which is 100 m above mean sea level).

is not well defined: some billows also existed outside the envelope in Figure 2. The relationship of the billow patch to MCS B's rain area is shown in Figure 1, where the white lines represent the locations of the billow patch interpolated from the envelopes in Figure 2. The patch of billows was travelling from about 235° at between 7 and 10 m s^{-1}, and it maintained its position within the region of mainly moderate rain that was trailing behind MCS B.

2.2. *Structure of the billows*

Figure 3 shows RHI plots from the Chilbolton radar for the single scan along 348° through the middle of the billow patch at 1023. This scan was roughly parallel to, and to the west of, the north–south line of heavy convective rain cells that characterized the leading edge of MCS B. The scan encountered the region of relatively weak rain due to elevated convection at the rear of MCS B. The reflectivity plot in Figure 3(a) shows the weak convective precipitation extending upwards to about 6 to 8 km. The cells have a spacing of typically 2–4 km. Distinct cells are easily recognized at ranges out to 60 km; at greater ranges the cellular structure is evident mainly from the reflectivity streamers where they descend through the stably stratified air below the melting level at 3.3 km. The strong tilt of these streamers is due to the strong environmental shear below about 3 km. In the convective layer above 3 km the shear was quite small.

Figure 3(b), depicting the Doppler velocity, shows the inclined layer of strong shear within which the billows formed: the centre of the layer can be seen sloping upwards from about 2 km at 40 km range to about 3.8 km at 95 km. Figure 3(c) shows the Doppler shear derived from Figure 3(b). At the low elevation angles involved, the Doppler shear is essentially the vertical shear of the horizontal wind (resolved along 348°). As shown by Chapman and Browning (1998), for a radar with a narrow beam, Doppler shear plots are a particularly effective way of identifying KH billows, and these are evident from the orange-red braided echo patterns in Figure 3(c).

The spectral width in Figure 3(d) is essentially the sum of contributions from turbulence and the vertical shear component across the beam width. The 0.28° beam of the Chilbolton radar gives a width of about 300 m at 60 km and so regions with a shear of over 0.02 s^{-1} correspond to a 6 m s^{-1} range of velocities across the beam, suggesting that the shear was the dominant contributor to the spectral width measured in the billows. It is therefore not surprising that the pattern of high spectral width in (d) is broadly similar to the pattern of high shear in (c).

The braided echo patterns seen in Figures 3(c) and (d) within the strongly sheared layer resemble the large-amplitude billows observed in clear-air reflectivity patterns by Browning and Watkins (1970) and in wind shear patterns in an area of frontal precipitation by Chapman and Browning (1997). The crest-to-trough amplitude of the billows in the present case is seen to be 500–700 m at ranges between 50 and 60 km. Billow amplitudes are about half this value at closer ranges. Beyond 70 km, quasi-horizontal filaments can be seen. These filaments are similar to those observed by Browning and Watkins (1970), who demonstrated that they corresponded to split shear layers left over after billows had broken. Alternatively, the filaments in the present case may have been due to pre-existing or previously split shear layers.

Above the billows, in the layer between 5 and 7 km altitude, Figure 3(c) shows slanting (cyan and green/yellow) oscillations in wind shear, especially beyond the 70 km range. The cause of these is not understood but they are not the main subject of this study. They may perhaps have been due to gravity waves forced by the MCS convection or by the billows themselves, which appear to have a broadly similar wavelength. However, if they were indeed gravity waves, this would suggest that the convective precipitation

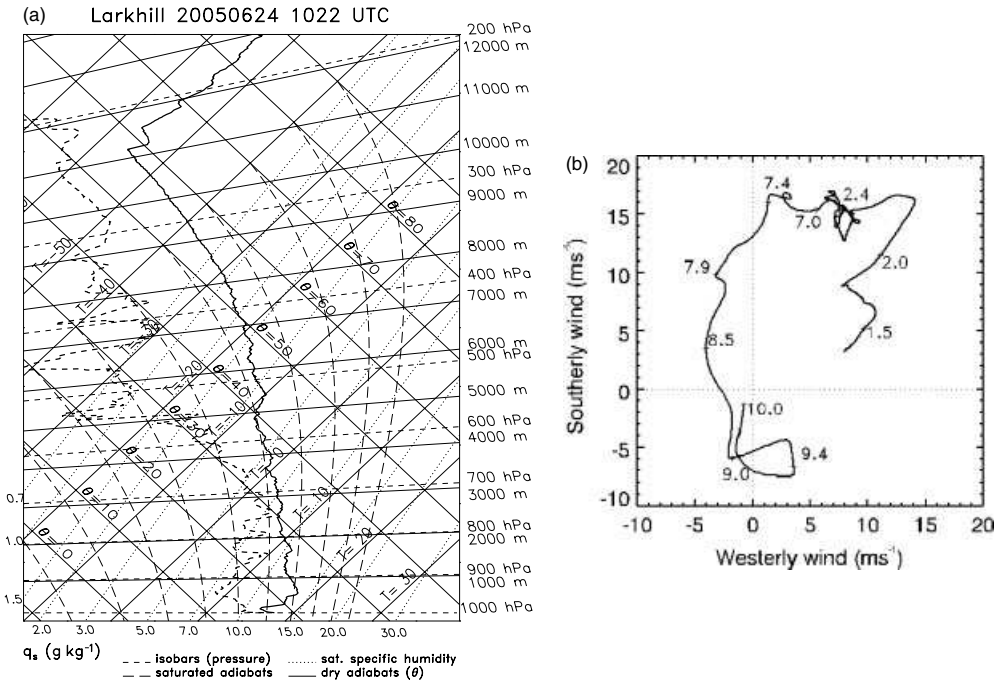

Figure 4. Sounding data from the Larkhill radiosonde ascent at 1022 UTC, 24 June 2005: (a) tephigram (with dashed lines showing constant pressure levels and solid lines showing constant heights above mean sea level) and (b) hodograph (pressure labelled in units of 100 hPa).

seen at these levels (Figure 3(a)) was due to convection that had largely ceased by the time of this radar scan, since a saturated adiabatic profile through active convection is not conducive to gravity wave propagation. Slanting oscillations in wind shear are not evident below the billows, but the near-horizontal layering of both the wind shear (cyan and green/yellow layers in Figure 3(c)) and the spectral width (grey and blue layers in Figure 3(d)) is consistent with static stability and the absence of convection in the underlying cool air (i.e. in what we call the 'undercurrent').

2.3. Vertical structure of the atmosphere in the vicinity of the billow patch

A radiosonde was released from Larkhill at 1022, corresponding closely in time and space to the RHI scan in Figure 3. Its location is denoted by the '+' sign labelled 'L' in Figure 2, which puts it about 20 km south of the main billow patch, i.e. at a radar range of about 20 km in the RHI scan in Figure 3. The RHI scan shows that the height of the shear layer with which the billows were associated decreased towards the radiosonde site, at which location it would have extended between about 1 and 2 km (i.e. 900–800 hPa). The tephigram for the Larkhill ascent, in Figure 4(a), shows that this layer corresponded to a moderately stable layer at the top of the cool undercurrent. The Larkhill wind hodograph, in Figure 4(b), confirms the existence of strong shear between 800 and 900 hPa. Since the shear vector over this height interval was orientated along 355°, i.e. within 7° of the direction of the RHI scan in Figure 3, we can make a direct comparison between the shear observed by the radar and the shear observed by the radiosonde. The hodograph in Figure 4(b) shows a shear vector of 15 m s^{-1} between 900 and 790 hPa. According to the Chilbolton radar, much of this velocity change was concentrated within a height interval of 300 m in parts of the billows (orange-red areas in Figure 3(c)).

Because the RHI scan in Figure 3 was orientated along the main shear vector, we can also interpret the observed wavelength of the billows as being a measure of their true wavelength. The largest billows, between 50 and 60 km range, are seen to have had a wavelength of 4 km and a crest–trough amplitude of 700 m. The resulting wavelength/amplitude ratio of 6 is in the middle of the range of values for this ratio found in the study of 16 atmospheric KH billow events by Browning (1971).

Miles and Howard (1964) concluded on the basis of theoretical computations that, for a linear profile, the fastest-growing billows should have a wavelength between 4.4 and 7.5 times the thickness of the initial shear layer. Although this theoretical result depends strongly on the shapes of the velocity and density profiles, it suggests that the largest billows in the present case may have been triggered by a layer roughly 500–900 m thick, i.e. corresponding to a large part of the strongly sheared layer between 900 and 790 hPa shown in Figure 4(b). Smaller-amplitude billows observed elsewhere within the billow envelopes shown in Figure 2 tended to have shorter wavelengths, consistent with the shearing instability occurring over a shallower layer.

2.4. Surface pressure perturbations beneath the billows

The edge of the billow patch passed over the AWS installed at North Farm (small square labelled N in Figure 2) between 0945 and 1100. Figure 2 suggests that this AWS may have been well within the billow envelope only for the latter part of the period, from 1023 to 1100. Figure 5 shows traces of surface pressure, temperature, relative humidity, wind speed and wind direction at N between 1000 and 1200. There were evidently no short-term fluctuations in either temperature or humidity at the surface and the surface wind was less than 1 m s^{-1} throughout the period up to 1100; however, there were rapid fluctuations in pressure between 1027 and 1100. The pressure fluctuations had amplitudes of up to ± 0.3 hPa and a period of about 9 min. The time of occurrence of these fluctuations suggests that they may have been due to the billows, presumably a result of the hydrostatic effect from overlying temperature anomalies caused by the billows displacing air parcels vertically within the statically stable layer in which they were embedded.

To test the hypothesis that the billows could have been responsible for the periodicity of the observed fluctuations in surface pressure, we first need to estimate the wavelength implied by the 9 min period of the fluctuations. The hodograph in Figure 4(b) suggests that the speed at which the billow troughs and peaks can be expected to have advected over the AWS was 4 m s^{-1} (or less/more), depending on whether the midpoint of the billow layer was associated with the 850 hPa (or a lower/higher) level within the hodograph. Assuming an advection velocity of 4 m s^{-1}, the 9 min period of the pressure fluctuations in Figure 5 would correspond to the passage of billows of wavelength about 2 km, i.e. less than that of the large-amplitude billows seen between 50 and 60 km range in Figure 3 and more like that of the smaller billows observed elsewhere in the billow patch. Such small billows would be expected to have had crest–trough amplitudes of only about, say, 300 m. Assuming that the observed surface pressure anomalies of ± 0.3 hPa were indeed hydrostatic effects due to the overlying billows, this would imply mean temperature anomalies of ± 1° C over the 300 m depth of the billows. This is not unreasonable since Figure 4(a) shows that the potential temperature increased by 4°C km^{-1} over the layer 900–800 hPa, with embedded layers having vertical gradients in excess of this.

3. Observations relevant to the structure and behaviour of elevated convection above the billows

3.1. Effect of deepening undercurrent on elevated convection

The shear layer marked the transition from a cool northerly undercurrent flow to an overrunning warm and potentially unstable southerly flow. The sounding in Figure 4(a) shows that air parcels with high wet-bulb potential temperature (θ_w) at 750 hPa, given about 150 hPa of initial lifting to reach their level of free convection, would have been able to ascend with a small amount of buoyancy to about 550 hPa. With some lifting of the drier air above 750 hPa, buoyant convection to 550 hPa and above would have been possible with much less initial lifting of the high-θ_w air. As shown by Figure 3(a) (and Figure 6 later), convection did in fact occur up to and above the 500 hPa (6 km) level. As we now show, there is evidence for the existence of the broad-scale lifting required to initiate that convection.

The broad-scale lifting was associated with the observed major deepening of the undercurrent towards the north, which can be seen in Figure 3(b) from the slope of the strongly sheared layer at the top of the undercurrent.

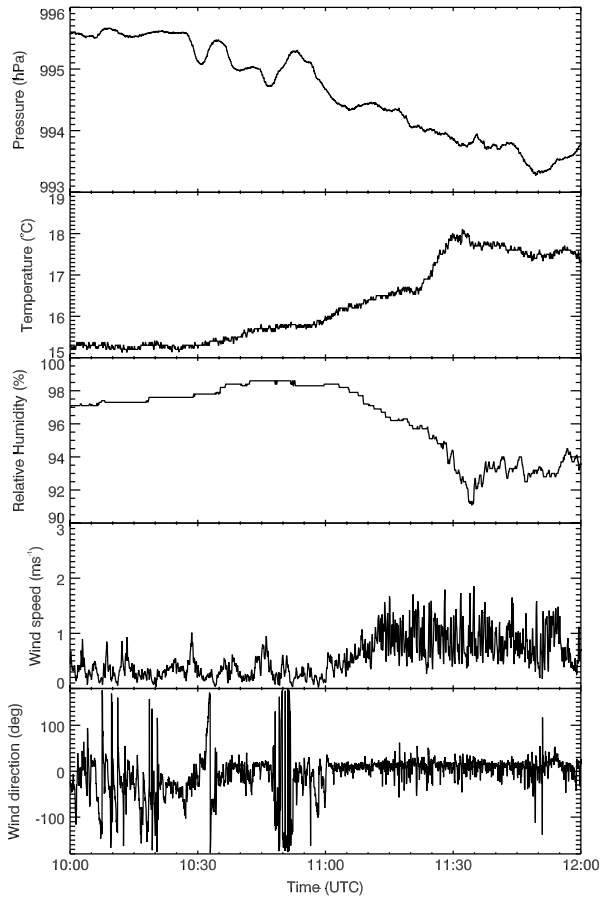

Figure 5. Data from the North Farm automatic weather station (N in Figure 2) for the period 1000–1200 UTC, 24 June 2005, showing pressure, temperature, relative humidity, wind speed and wind direction.

Figure 4(b) shows that the high-θ_w air at 750 hPa that would have fed the elevated convection had a stronger southerly component than air within the shear layer. Since the shear layer was observed to maintain its slope over time, the high-θ_w air would have ascended, from left to right in Figure 3, above the inclined shear layer at the top of the undercurrent. Source air for the elevated updraughts, in travelling northwards from the location of the Larkhill sounding, would therefore have ascended as much as 1 km by the time it reached the centre of the billow area (at a range of around 60 km in Figure 3). Since the broad-scale lifting would to some extent also have affected (and cooled) the drier air just above the high-θ_w air, it is not surprising that the elevated convection was being triggered. This would have occurred with or without the presence of the underlying billows.

What caused the slope in the depth of the undercurrent is not clear. It will have been influenced by the presence of a broad baroclinic zone in which the MCSs were situated, as discussed in Browning *et al.* (2010). It was probably also influenced by the combined effects of MCS B and another MCS behind it. It has been shown by Marsham *et al.* (2010) that gravity waves associated with another MCS on this day caused considerable variation in the depth of the undercurrent near the core of that MCS, as well as strengthening the shear and triggering billows behind the storm. In that case, the billows were observed near where the depth of the undercurrent was *reduced* by an impacting rear-inflow jet; in the present case, however, the billows occurred in an area where the undercurrent was *deepening*. The major deepening of the undercurrent that led to the elevated convection in the region of the billow patch being discussed in this paper is therefore more likely to have been due to the larger-scale dynamics associated with the broad baroclinic zone.

3.2. *Relationship of the elevated convection to the billows*

We have just shown that the elevated convection would most likely have occurred even in the absence of the billows, but that is not to say that the convection was not also affected by the billows. We now show data from a RHI scan that does suggest some interaction.

We suggested earlier that the precipitation cells seen in Figure 3 were probably due to elevated convection that might have ceased by the time of the RHI scan in that figure. One of the RHI scans that most clearly depicts *ongoing* convection above the billow patch was obtained along 025° at 1052 (Figure 6). Figure 2 shows that this scan went through the billow patch at its eastern boundary, and in a region where the convection was still active; however, a disadvantage of the scan is that the billows were less clearly defined here. According to Browning *et al.* (2010), it is sometimes possible to discern the boundaries of convective plumes rising within a region already filled with precipitation echo, from the enhanced Doppler spectral width at their boundaries. Such is the case in Figure 6(c), which shows five broad convective 'plumes' rising to between 5 and 6 km, centred at ranges 48, 63, 73, 84 and 91 km. There are also faint outlines of parts of 'plumes' extending even higher, to 8 km, at

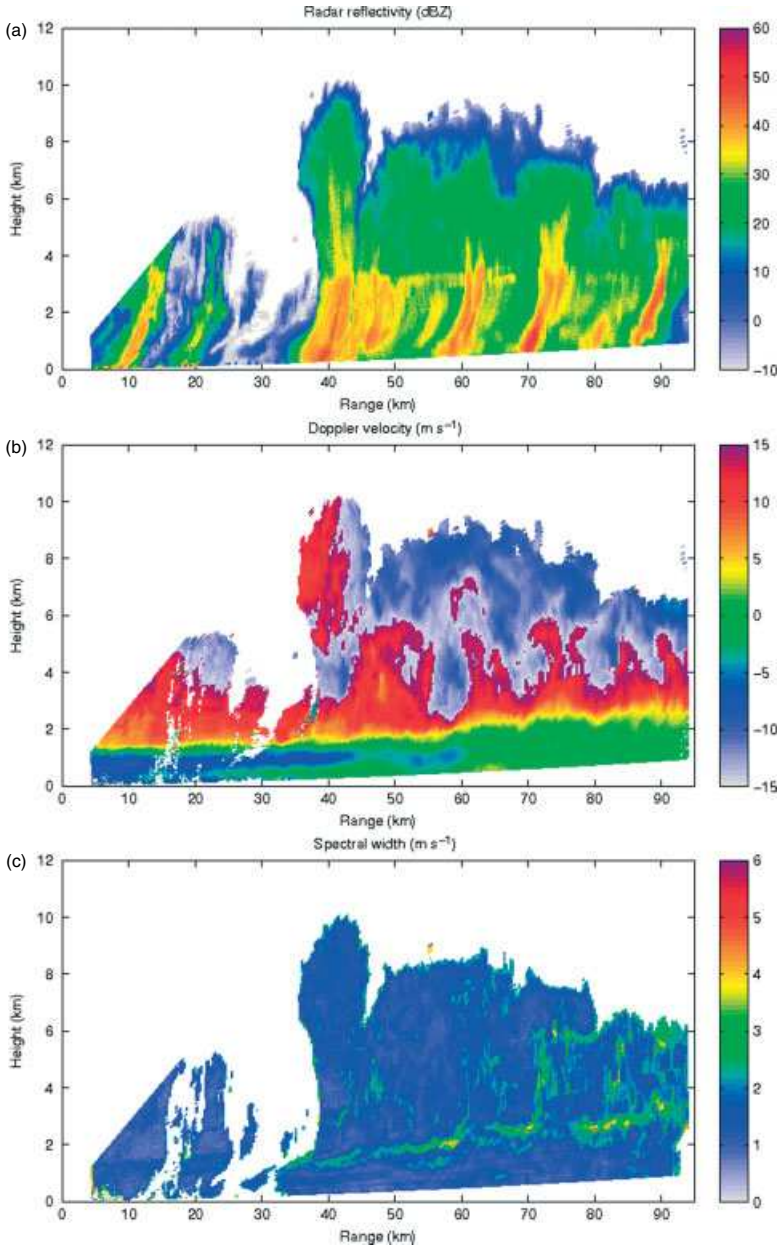

Figure 6. RHI scan from the Chilbolton radar along 025° at 1052 UTC, 24 June 2005, showing (a) reflectivity, (b) Doppler velocity (velocities are 'folded' such that the upper grey and blue areas represent positive velocities greater than 15 m s^{-1}) and (c) spectral width. As Figure 3, heights are above the radar dish.

around 62 km. These 'plumes' are each 5–12 km wide and so what we are referring to as 'plumes' were probably clusters of individual convective plumes. These aggregate plumes also show up in the Doppler velocity image in Figure 6(b) as regions of lower-velocity air (red) brought up from lower levels and penetrating into higher-velocity air (grey and blue). Figure 6(a) shows that each aggregate plume was responsible for a local maximum in precipitation intensity, with evidence of substructure due to streamers from individual convective sub-cells about 2 km wide.

The convective 'plumes' originated from just above the level of the main shear layer within which the billows were occurring. Specifically, Figure 6(c) shows that the sheaths of higher spectral width due to turbulence at the 'plume' boundaries emanate from the layer of high spectral width due to the main shear layer, which slopes upwards from 1.4 km at 40 km range to 3.2 km at 90 km. This corresponds to the strongly sheared layer within which the billows developed, although the billows in this scan are poorly organized. As suggested above, the poor organization of the billows here may be because the scan was through the edge of the billow patch. One of the better-defined billows, which can be seen in Figure 6(c) at ranges between 60 and 67 km, appears to be connected to one of the overlying convective 'plumes', suggesting the possibility that the billows were helping to trigger the convection and/or the convection was facilitating the development of the shearing instability.

The tephigram in Figure 4(a) shows that, although air with the highest θ_w was located at 750 hPa, well above the strongly sheared layer, there were also other moist layers with moderately high θ_w at 790 hPa (i.e. just at the top of the shear layer), and at 840 hPa (actually within the shear layer). It is possible that air from these layers became entrained into the overlying updraughts when the billows broke and this might account for the way in which the boundaries of

the convective plumes in Figure 6(c) appear to originate in the shear layer within which the billows formed.

4. Results from the large-eddy model relating to interaction of billows and overlying convection

4.1. Model configuration

To investigate the interaction between the billows and the convection, a set of two-dimensional model runs was established using version 2.4 of the Met Office Large Eddy Model (LEM) (Derbyshire *et al.*, 1999; Gray *et al.*, 2001). The LEM is a non-hydrostatic model, which solves an anelastic quasi-Boussinesq set of equations. A horizontal grid spacing of 100 m was used, with a stretched vertical grid, which had a grid spacing of approximately 25 m at the level of the billows. The model was run with prognostic single moment (mass) cloud and rain, and double moment ice, snow and graupel (mass and number). Each run was initialized using the Larkhill 1022 UTC profiles of temperature, moisture (Figure 4(a)) and north–south wind component (Figure 4(b)). As explained in section 2.3, the layer in which the billows developed was between 900 and 800 hPa at the location of the Larkhill sounding. It can be seen from Figure 4(b) that the shear vector over this layer was orientated almost north–south, so that the modelled cross-section captures most of the relevant shear.

In order to simulate the environment in which the billows were observed to form, large-scale ascent was imposed in all model runs. The LEM uses periodic boundary conditions and so, because mass cannot be moved in or out of the model domain, ascent could not be forced directly. Instead, the effects of large-scale ascent were simulated by forcing the temperature, water vapour and winds. The forcings that were applied corresponded to zero rate of ascent at the surface and 20 cm s^{-1} above 2 km; between these heights the ascent rate was interpolated linearly. All model runs were initialized identically, the ascent being applied from 1.5 h into each run, i.e. starting after the completion of spin-up in all the runs.

Three LEM simulations were performed, with each run using a different forcing of the mean wind profile. In the control run, referred to as the 'observed shear' run, the horizontally averaged winds were relaxed to the observed wind profile (after adjusting for the imposed ascent). This effectively controlled the mean wind profile while maintaining perturbations from it. This run developed convective plumes but, at a time corresponding to an imposed ascent of order 1 km, billows were much less developed than those observed. In order to study the effects of larger billows, winds in a second run, were relaxed to $(1 + 0.1t)$ times the observed wind profile, where t is the simulation time in hours. This run, referred to as the 'increasing shear' run, generated large billows as the convection formed. Finally, in order to prevent the generation of any billows, a 'low-shear' run was also performed, with horizontally averaged winds relaxed to zero. We first show, in Figure 7, the structure of the realistic billows and convection that we were able to reproduce in the 'increasing shear' run, and then go on to compare, in Figure 8, the temporal evolution of the structures that developed in the three different runs.

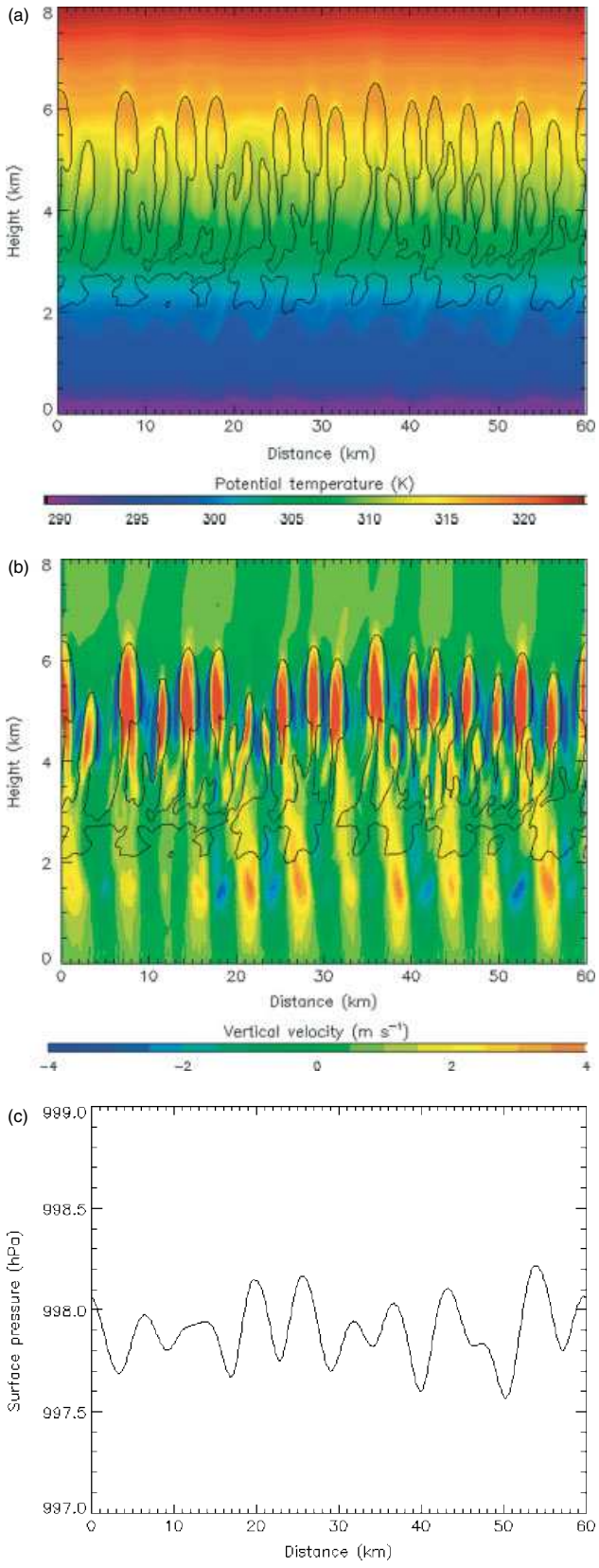

Figure 7. Model fields from the 'increasing shear' run at 9450 s, after a total uplift of 810 m. Coloured cross-sections show potential temperature in (a) and vertical velocity in (b), with lines showing cloud (total hydrometeor content > 0.5 g kg^{-1}). Surface pressure is shown in (c).

4.2. Model results

Figure 7 shows vertical cross-sections after 810 m of ascent, shortly after the large billows had developed in the

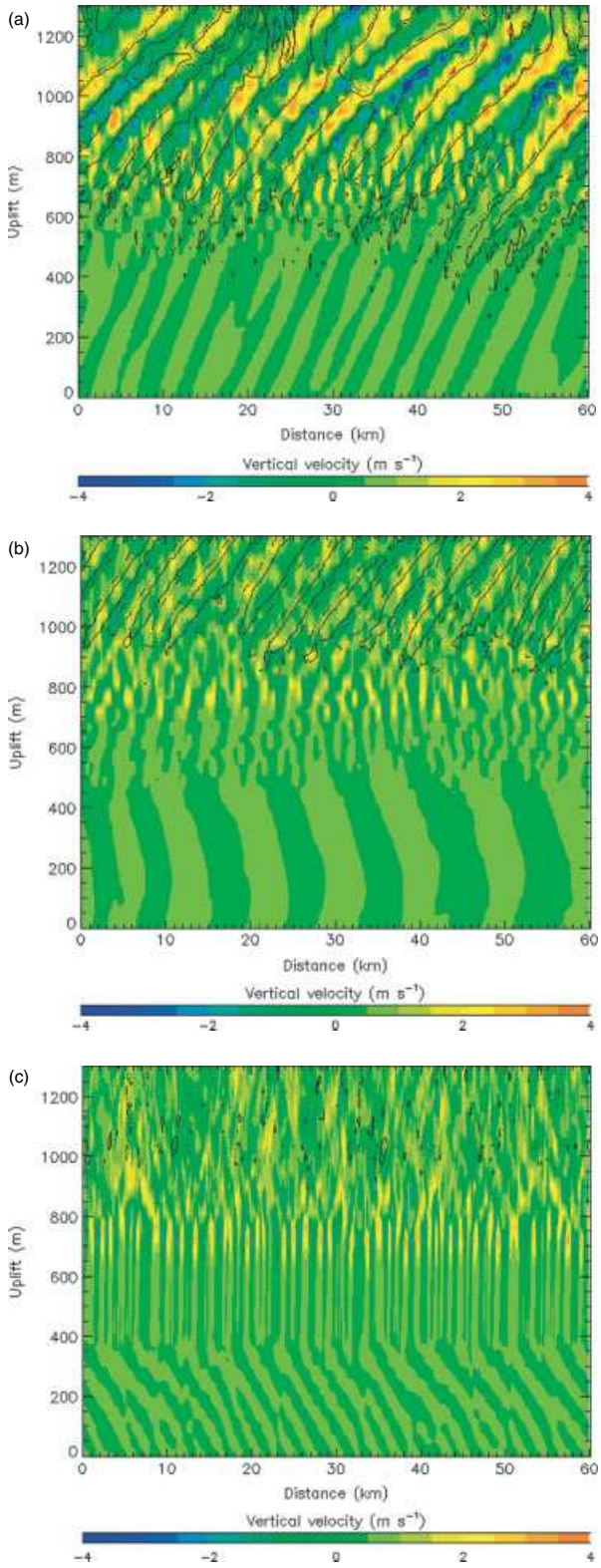

Figure 8. Hovmöller (time–distance) plots, with the time axis expressed in terms of effective uplift, showing vertical velocity at 3.5 (coloured) and 1.5 km (solid/dashed lines at $\pm$ 0.5 m s^{-1}) for (a) the 'increasing shear' run, (b) the 'observed shear' run and (c) the 'low shear' run.

'increasing shear' run. Figures 7(a) and (b) show potential temperature and vertical velocity, respectively, along with an outline of the clouds (defined by a total hydrometeor content of 0.5g kg^{-1}). The billows, highlighted by the transition from dark blue to light blue in Figure 7(a), are seen to be centred at a height of 1.8 km. This is equivalent to a height of approximately 2.6 km after including the imposed ascent, i.e. similar to the observations. The billows have crest-to-trough amplitudes of about 500 m and a wavelength of 5–6 km. These values are broadly compatible with the maximum observed crest-to-trough amplitude of up to about 700 m and wavelength of about 4 km. Figure 7(c) shows that modelled surface pressure perturbations at this time are up to $\pm$ 0.3 hPa, again broadly consistent with the observations (Figure 5).

Figures 7(a) and (b) show that billow clouds form at the crest of each of the billows, centred at a height of about 2.3 km, equivalent to 3.1 km. Convective clouds form above the billow clouds and reach heights of 6.5 km (equivalent to 7.3 km); this is again consistent with the 5–8 km tops of the plumes observed in Figure 6. Figure 7(b) shows that, above 5 km (5.8 km), the convective updraughts are 2–3 km wide, which is comparable to that observed for the individual plumes but narrower than the aggregate plumes; however, in the lower parts of the convective clouds, around 3.5 km (4.3 km), the updraughts have a width more nearly comparable with, but still less than, that of the observed aggregate plumes (5–12 km). In the 'observed shear' run (not shown), undulations from developing billows are just visible in the shear layer at around 1.75 km at this time, with some of these forming small billow-crest clouds centred at 2.5 km. The convective clouds in this run extend up to 6 km. In the 'low shear' run (not shown), where there were no billows, deep convection forms as in the other runs, but their structure differs in detail.

The modelled impact of the billows on the convection is seen in Figure 8. This shows Hovmöller plots of the vertical velocities at 1.5 km (2.3 km), within the shear layer in which the billows develop (line contours), and at 3.5 km (4.3 km), in the lower part of the layer where the elevated convection develops (colours). Initially, i.e. for small uplift, the 3.5 km level is actually above any convection. Figure 4(a) shows that, above the clouds, the atmosphere is stable with respect to vertical displacements that do not lead to saturation, and so the velocity fluctuations at 3.5 km are due initially not to convection but to gravity waves. This is so for all three runs. Cross-sections similar to that in Figure 7 but at earlier times (not shown) reveal that the gravity waves are slightly inclined to the vertical, although not to the extent of the waves that were inferred from the observations to have existed above 4 km – see the earlier discussion of Figure 3(c).

The coloured shading in Figure 8 shows that, in all three runs, after about 400–500 m of uplift, the top of the convection rises sufficiently for the convective updraughts to take over from the gravity waves at the 3.5 km (4.3 km) level. The line contours in Figure 8 show that, at a height of 1.5 km (2.3 km), billow updraughts first become apparent after about 500 and 900 m of uplift in the 'increasing shear' and 'observed shear' runs, respectively (Figures 8(a) and (b)). In these runs *the updraughts in the elevated convection at 3.5 km (4.3 km) become locked to the billows as soon as the billows become apparent.* Before the billows develop, the updraughts in the convectively unstable layer have a much smaller spacing than the billows. Therefore the modelled billows appear to increase the spacing of the modelled convection from approximately 3 km to 7.5 km at the 3.5 km (4.3km) level, i.e. to something closer to the 5–12 km scale of the observed aggregate plumes. However, Figure 7(b) shows that the tops of the convection retain a smaller spacing,

consistent with the observed existence of sub-structure in the aggregate plumes.

As the billows themselves develop in the 'increasing shear' run (Figure 8(a)), they increase their mean spacing a little, from 6 to 7.5 km. This small change may be due to the effect of the developing convection or it might have happened in any case without the convection.

As pointed out earlier, the Larkhill sounding in Figure 4(a) shows that there were three layers of high-θ_w air, some or all of which may have contributed to the elevated convection. Tracer transport to upper levels from each of these layers in the LEM (not shown) was found to be similar in all three runs, including the 'low shear' run (Figure 8(c)) in which billows did not form. Therefore the modelled impact of the billows on convection was not a result of the billows making more layers of high-θ_w air available to the convection; instead it must have been solely a result of the vertical-velocity forcing provided by the billows. These idealized simulations do not rule out the possibility of the billows having made more layers of high-θ_w air available to the convection in the observed case; rather, they demonstrate that the billows may have modulated the convection even if this did not occur.

5. Conclusions

We have presented a case study of an event in which an extensive area of KH billows occurred at the sheared boundary between a surface-based cool air mass and an overlying region of potentially unstable air that was giving rise to mesoscale convective systems. KH billows, especially when they have large amplitudes as on this occasion, are important for their role in mixing and as a turbulence hazard for aviation. The billows occupied an area of 2000 km^2 and propagated at about the same velocity as the MCSs with which they were associated, persisting for more than 2 h. They occurred in an area of moderate rainfall intensity behind the leading region of intense convection associated with one MCS and ahead of another, weaker MCS, but the causal relationship is not understood.

The statically stable shear layer in which the billows were embedded was tilted. It rose from a height of 1.8 km to 3.6 km over a distance of 70 km in a roughly northerly direction, corresponding to the direction of the shear. Potentially unstable air ascended slantwise in a roughly northerly direction above this layer, giving rise to the elevated convection. The observed elevated convection was in the form of plumes or aggregates of plumes many kilometres across. Although the large-scale ascent alone would have been sufficient to trigger the elevated convection, the observations show that the aggregate convective plumes emanated from the shear layer in a way that suggested an interaction between billows and the convection. A set of three simulations using a two-dimensional large-eddy model, driven by a representative observational sounding but with varying strengths of shear, supports the view that the vertical velocities associated with the billows had a forcing effect on the convection. The development of the billows in the model appeared to influence (increase) the horizontal scale of the elevated convection. Possibly the scale of this forcing above the larger billows was such as to cause individual convective plumes, about 2 km across, to cluster together to form the larger 'aggregate plumes'.

Acknowledgements

The original CSIP project and the extended analysis phase leading to the present paper were funded under grants by the Natural Environment Research Council (NERC:NER/O/S/2002 00971 and NE/B505538/1). Special thanks are due to the many who participated in the CSIP field programme, in particular Barbara Brooks (University of Leeds), who deployed the AWSs. The Chilbolton Observatory, around which the project was based, is owned by the Science and Technology Facilities Council. Data from the weather radar network and the additional Larkhill radiosonde were provided by the Met Office. We would like to thank two anonymous reviewers, whose comments have improved the clarity of the paper.

References

Browning KA. 1971. Structure of the atmosphere in the vicinity of large-amplitude Kelvin–Helmholtz billows. *Q. J. R. Meteorol. Soc.* **97**: 283–299.

Browning KA, Watkins CD. 1970. Observations of clear air turbulence by high power radar. *Nature* **227**: 260–263.

Browning KA, Blyth A, Clark P, Corsmeier U, Morcrette C, Agnew J, Ballard S, Bamber D, Barthlott C, Bennett L, Beswick K, Bitter M, Bozier K, Brooks B, Collier C, Davies F, Deny B, Dixon M, Feuerle T, Forbes R, Gaffard C, Gray M, Hankers R, Hewison T, Kalthoff N, Khodayar S, Kohler M, Kottmeier C, Kraut S, Kunz M, Ladd D, Lean H, Lenfant J, Li Z, Marsham J, McGregor J, Mobbs S, Nicol J, Norton E, Parker D, Perry F, Ramatschi M, Ricketts H, Roberts N, Russell A, Schulz H, Slack E, Vaughan G, Waight J, Watson R, Webb A, Wareing D, Wieser A. 2007. The convective storm initiation project. *Bull. Am. Meteorol. Soc.* **88**: 1939–1955.

Browning KA, Marsham JH, Nicol JC, Perry FM, White BA, Blyth AM, Mobbs SD. 2010. Observations of dual slantwise circulations above a cool undercurrent in a mesoscale convective system. *Q. J. R. Meteorol. Soc.* **136**: 354–373.

Chapman D, Browning KA. 1997. Radar observations of wind-shear splitting within evolving atmospheric Kelvin-Helmholtz billows. *Q. J. R. Meteorol. Soc.* **123**: 1433–1439.

Chapman D, Browning KA. 1998. Use of wind-shear displays for Doppler radar data. *Bull. Am. Meteorol. Soc.* **79**: 2685–2691.

Derbyshire SH, Brown AR, Lock AP. 1999. The Meteorological Office large-eddy simulation model. *Turbulence and Diffusion Note 213*, Met Office, Exeter, UK.

Goddard JFW, Eastment JD, Thurai. 1994. The Chilbolton advanced meteorological radar: a tool for multidisciplinary research. *Elect. Commun. Eng. J.* **6**: 77–86.

Gray MEB, Petch J, Derbyshire SH, Brown AR, Lock AP, Swan HA. 2001. Version 2.3 of the Met Office large-eddy model. *Turbulence and Diffusion Notes 275–277*, Met Office, Exeter, UK.

Harrison DL, Driscoll SJ, Kitchen M. 1998. Improving precipitation estimates from weather radar using quality control and correction techniques. *Observation based products technical report No. 13*, Met Office, Exeter, UK.

Houser JL, Bluestein HB. 2011. Polarimetric Doppler radar observations of Kelvin–Helmholtz waves in a winter storm. *J. Atmos. Sci.* **68**: 1676–1702.

Marsham JH, Browning KA, Nicol JC, Parker DJ, Norton EG, Blyth AM, Corsmeier U, Perry FM. 2010. Multi-sensor observations of a wave beneath an impacting rear-inflow jet in an elevated mesoscale convective system. *Q. J. R. Meteorol. Soc.* **136**: 1788–1812.

Miles JW, Howard LN. 1964. Note on a heterogeneous shear flow. *J. Fluid Mech.* **20**: 331–336.

